# Development of a line-scan CCD-based fringe tracker for optical interferometry

Agustí Pintó and Ferran Laguarta

Traditional high-precision optical techniques, such as interferometry, are in ever-greater demand for noncontrolled environments. This is the case for the UPC-ZEBRA, a large-aperture interferometer that was built to measure vertical discontinuities (i.e., piston errors) in segmented mirrors. The large mechanical systems used to drive the interferometer to the different measurement positions generate perturbations that are highly incompatible with the expected piston measurements on the nanometer scale. We introduce a new system based on a line-scan CCD to track interference fringes. The error signal obtained from this fringe tracker has been used in a closed-loop control system to actively stabilize the interferometer. The perturbation has been attenuated by a factor of 1/200. 

*OCIS codes:* 120.3180, 120.3930.

## 1. Introduction

Many techniques that were once restricted to laboratory use are now in demand for use in less favorable conditions such as industrial environments. One such technique is optical interferometry. Many interferometry applications require vibration isolation conditions that in most cases are not satisfied. Therefore an auxiliary system is needed to actively or passively compensate for the perturbations.

A typical active control system consists of a detector that provides a signal of the magnitude to be controlled. This signal is compared to a reference value, and an error signal is extracted by subtracting these values. The error signal is fed to a control stage that outputs the control signal to an actuator to keep the magnitude at the desired value.

The error signal extraction technique is a key element in active vibration stabilization in interferometry. Several techniques have been developed to extract perturbation in interferometers for use in gravitational wave detectors,[1–3] vibration control in spacecraft,[4] large optics testing,[5,6] and astronomical interferometry.[7–9] A detailed review of the techniques used for error signal extraction in optical interferometry can be found in Ref. 10.

In this work, we present, what is to the best of our knowledge, a new error signal extraction technique that is specifically designed to compensate for vibrations in the positioning system of the UPC-ZEBRA interferometer,[11,12] which was built to measure the segment piston in large segmented mirrors. As the measurement is carried out locally, a robotic arm is needed to sequentially position it in front of each pair of segments, whose piston needs to be measured (at a working distance of 10 cm). Given the mechanical characteristics of the positioning systems that are commercially available, the interferometer would be expected to oscillate with respect to the segmented mirror on a scale beyond the tolerances of the interferometer, thus making it impossible to take interferometric measurements.

The perturbations are expected to generate large optical path difference (OPD) oscillations in the low-frequency regime due to the large mass of the interferometer. A preliminary study revealed that these oscillations would have a maximum amplitude of $\pm 300$ μm and a frequency lower than 1 Hz. Because the system would probably be well outside of working conditions (i.e., OPD far from zero) and the oscillation frequency would be very low (pseudo-dc), modulation techniques could not be used to extract the vibration. We have developed a new technique that uses a high-frequency line-scan CCD camera to extract the perturbation.

The authors are with the Center for Sensors, Instrumentation and Systems Development (CD6), Technical University of Catalonia (UPC), Rambla Sant Nebridi 10, 08222 Terrassa, Spain. A. Pintó's e-mail address is pinto@oo.upc.edu.

Received 28 November 2005; revised 8 March 2006; accepted 5 April 2006; posted 28 April 2006 (Doc. ID 66243).

0003-6935/06/266694-08$15.00/0

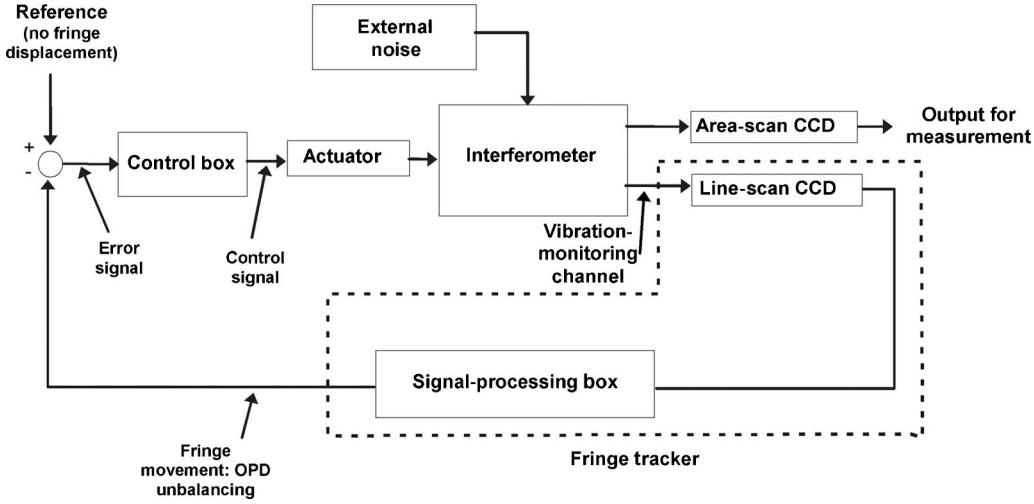


Fig. 1. Detailed control diagram.

We designed our technique specifically for a large-aperture Michelson interferometer for metrological use. We fully integrated the control system into the interferometer head as required by the environment in which it is designed to work.

Section 2 presents a detailed description of the error signal extraction technique. Section 3 presents the results of numerical simulations of the technique carried out using SIMULINK. Section 4 describes the optical setup developed to implement it, and Section 5 presents the preliminary experimental results. The conclusions are summarized in Section 6.

## 2. Description of the Technique

Most of the techniques that have been developed for extracting vibration in optical interferometers use high-speed point detectors such as avalanche photodiodes (APDs). The technique presented here parallelizes this approach by using a line-scan CCD camera. Recent developments in CCD arrays and increased computer power have made this method feasible. This technique has several advantages: It is a passive technique (i.e., no active modulation of the fringes is required) as it is not based on a point detector, and, as opposed to other passive techniques,[6] the fringe period does not have to match a predetermined period given by the geometry of the detector. Also, the fact of using a line-scan detector provides robustness to the technique due to the extended sampling of the interferogram.

A preliminary study showed that, using the expected perturbation described in Section 1, that is, large amplitude ($\pm 300$ μm) and pseudo-dc oscillation (less than 1 Hz), a capture frequency of at least 15 kHz was needed to properly sample the interferogram acquired by the line-scan CCD camera. Otherwise, while the line-scan CCD camera was acquiring the image, the interferogram would shift substantially, and the intensity detected by the line-scan CCD camera would be averaged, which would lead to a loss of contrast. Reference 10 contains a more detailed description of this point.

Today, several line-scan CCD cameras are commercially available that have a maximum capture frequency of 50,000 lines/s or more, which makes this approach technologically feasible. A fast computer is also required to process the data at the rate at which the line-scan CCD outputs them.

Figure 1 shows a diagram of the complete system, including the interferometer being perturbed by external noise, the fringe tracker, and the control-loop elements.

Our technique compares two consecutive interferograms acquired at a high frequency (high enough for the OPD change in the interval between the two interferograms to be less than a fourth of a fringe). After the signal is acquired by the line-scan camera, a signal-processing stage compares the current interferogram with the previous one and computes the OPD change (see Fig. 2). Together, the line-scan CCD camera and the signal-processing stage act as a fringe tracker. The fringe tracker's output is related to the OPD unbalancing caused by the perturbation. More precisely, it is proportional to the OPD change (or fringe velocity) in the interval between the two interferograms.

The following is a description of the algorithm used to compute the OPD change by comparing the consecutive interferograms. Let these interferograms be

- $I(\text{pixel}, t)$, the current interferogram, acquired at a time $t$.
- $I(\text{pixel}, t - \mathrm{d}t)$, the interferogram acquired before the current one at a time $t - \mathrm{d}t$. This interferogram is stored after acquisition.

The processing algorithm can be divided into two parts. In the first part, the modulus of the perturbation velocity is calculated, and in the second, its sign is extracted.

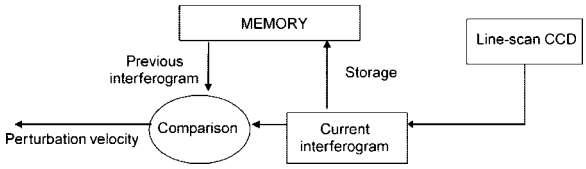

Fig. 2. Diagram showing the signal-processing algorithm.

The algorithm used to extract the modulus of the perturbation velocity first computes the difference in the intensity of the current interferogram and the previous one, pixel by pixel, and then adds all of these differences in absolute value. This value is defined as $h(t)$. Basically, this algorithm calculates the area between the two interferograms:

$$h(t) = \sum_{\text{pixels}} |I(\text{pixel}, t) - I(\text{pixel}, t - \mathrm{d}t)|. \quad (1)$$

By means of mathematical analysis, a relationship between this value and the OPD change can be obtained. In Appendix A to Ref. 10, a proof for the following relationship is provided:

$$h(t) = \frac{8NC\mathrm{d}t}{\lambda}\left|\frac{\mathrm{d}n(t)}{\mathrm{d}t}\right|, \quad (2)$$

where

- $N$ is the number of pixels of the line-scan CCD camera.
- $C$ is the contrast of the interference pattern, which depends solely on the lighting conditions.
- $\mathrm{d}t$ is the interval between the acquisition of the two consecutive interferograms. This value is the inverse of the acquisition frequency of the line-scan CCD camera.
- $\lambda$ is the wavelength of the light used.
- $|\mathrm{d}n(t)/\mathrm{d}t|$ is the absolute value of the perturbation velocity [we chose $n(t)$ to symbolize the perturbation, since it can also be considered noise].

The same information used to calculate the modulus is used to calculate the sign of the perturbation. The information on the sign of the perturbation is extracted from the relative intensities of two consecutive pixels at times $t$ and $t - \mathrm{d}t$. Let the intensities registered at these two pixels be those shown in Table 1.

The sign of the perturbation can be extracted by applying the following algorithm: compute (i) $I_i(t - \mathrm{d}t) - I_{i-1}(t - \mathrm{d}t)$ and (ii) $I_{i-1}(t - \mathrm{d}t) - I_{i-1}(t)$. If both (i) and (ii) have the same sign, the sign of the perturbation is positive; otherwise, the sign is negative.

This can be summarized in a single expression:

$$\mathrm{sgn}[\mathrm{d}n(t)/\mathrm{d}t] = \mathrm{sgn}\{[I_i(t - \mathrm{d}t) - I_{i-1}(t - \mathrm{d}t)] \times [I_{i-1}(t - \mathrm{d}t) - I_{i-1}(t)]\}. \quad (3)$$

To make the algorithm more robust, this calculation is repeated for several pairs of pixels. When more than 80% of the calculations yield the same result, the sign is considered correct, otherwise the computation is rejected, and the last known value for the sign is used.

**Table 1. Definition of Pixel Intensities at Different Times**

| | Pixel | |
|---|---|---|
| Time | $i$ | $i - 1$ |
| $t$ | $I_i(t)$ | $I_{i-1}(t)$ |
| $t - \mathrm{d}t$ | $I_i(t - \mathrm{d}t)$ | $I_{i-1}(t - dt)$ |

Then the final output of the signal-processing stage is

$$\frac{\mathrm{d}n(t)}{\mathrm{d}t} = \frac{\lambda}{8NC\mathrm{d}t}\, h(t) \times \mathrm{sgn}\left[\frac{\mathrm{d}n(t)}{\mathrm{d}t}\right]. \quad (4)$$

This signal can now be integrated over time to obtain the perturbation value. This is not required, however, because the perturbation velocity may be used as input in the control technique. The goal of the technique is to keep the input signal at zero, that is, the fringes at rest.

### 3. Numerical Simulation

To analyze the behavior of the error signal extraction technique, we ran several simulations. Some of these are presented here.

We modeled the complete system (interferometer plus fringe tracker) using the SIMULINK simulation software package. We carried out the simulation in a way that matched the real system closely. The only difference was that the interferograms were synthetically generated. However, the simulation did not take the effects of random noise (which might be caused by ghost reflections, CCD readout noise, or other sources) on the interferograms into consideration. The signal-processing stage was identical to the one used in the experiment.

Various types of perturbation may be applied to the interferometer during a simulation. We only present simulations with linear and sinusoidal perturbations here because the former is easy to analyze and the latter is the type expected in real operations.

Figure 3 shows the results of the simulation with a sinusoidal perturbation of $\pm 300$ $\mu$m amplitude at 0.5 Hz. Figure 3(b) shows that the error signal extraction technique recovers the perturbation over the full range with a maximum error close to 0.1% or 0.2 $\mu$m out of 300 $\mu$m. This value is good enough to stabilize the fringes. One inherent error of this technique is caused by the data-output time lag (one sampling period). This causes an error proportional to the perturbation speed at a given time. Other errors such as digital quantization also have an influence since the error found cannot be attributed exclusively to the time lag.

Figure 4 shows the results of the simulation for a linear perturbation of 1.6 $\mu$m/s. This simulation is particularly interesting because we acquired experi-

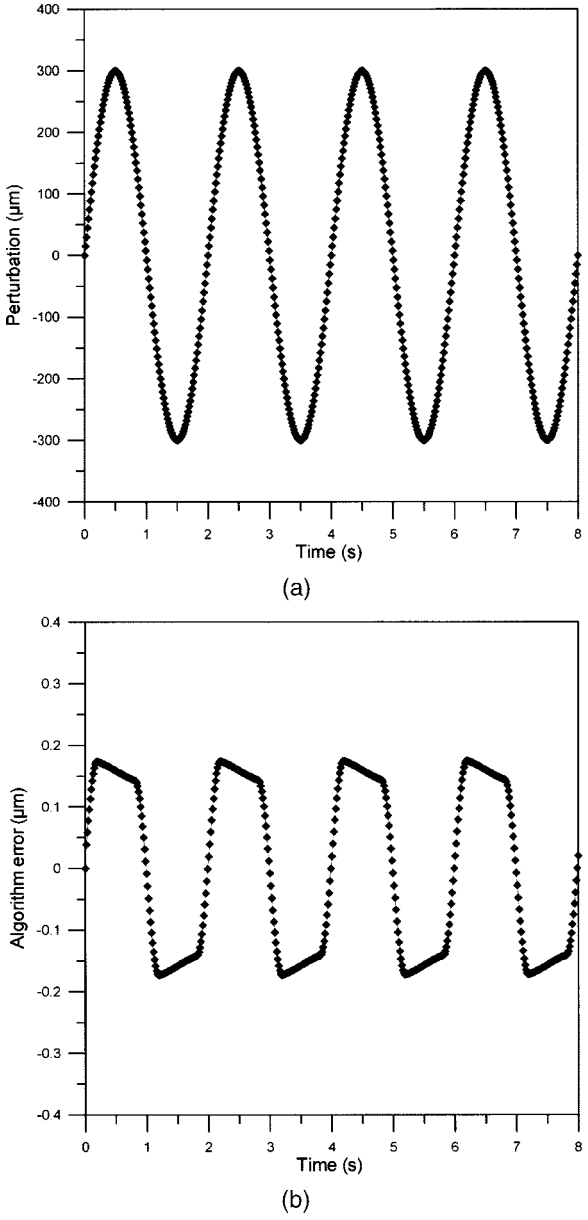


Fig. 3. Results of the simulation for a sinusoidal perturbation of ±300 μm amplitude at 0.5 Hz: (a) perturbation introduced and (b) residual error (extracted perturbation minus perturbation). The sampling frequency was 50 kHz.

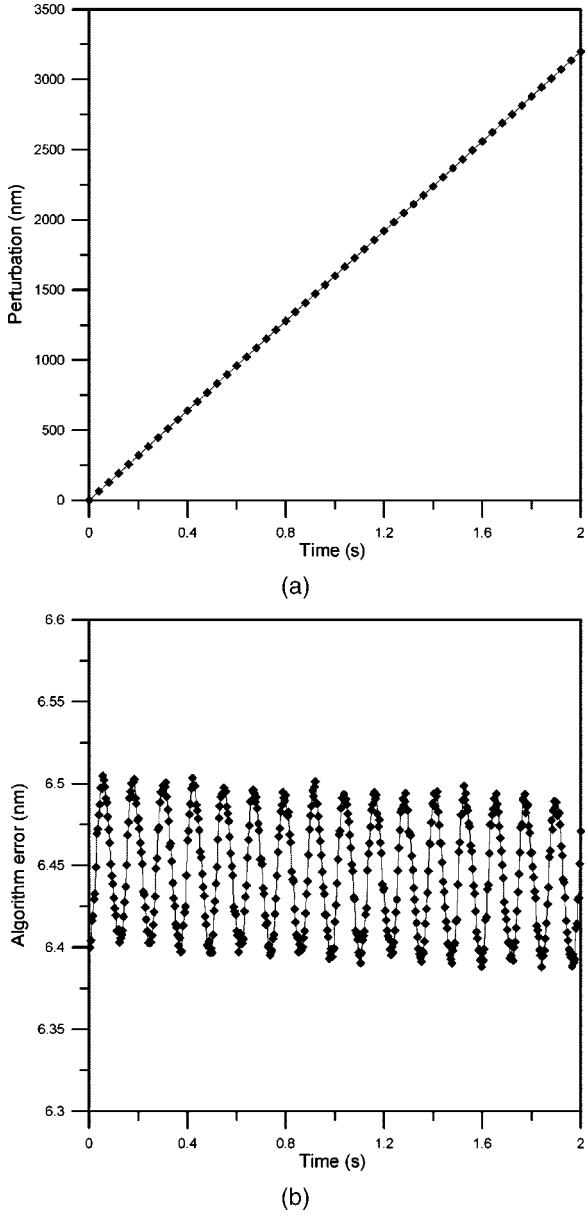


Fig. 4. Results of the simulation for a linear perturbation of 1.6 μm/s: (a) perturbation introduced and (b) residual error (extracted perturbation minus perturbation). The sampling frequency was 250 Hz. Please note that the vertical scale is now in nanometers.

mental data under the same conditions, which makes direct comparison possible (see Section 5).

Figure 4(b) shows that if the only factor that contributed to the algorithm error had been the time lag, we would have found a steady error because the perturbation speed is constant. This was not the case, although the error was very close to constant. By considering a linear perturbation of 1.6 μm/s and a sampling frequency of 250 Hz, we found that the error introduced by the time lag was 6.4 nm, in accordance with the value found in the simulation. However, as mentioned above, other sources of error, such as digital sampling, can have an influence (albeit a limited one) on the performance of the algorithm.

This ensures that the level of digital noise introduced by the algorithm is sufficiently low. After running the simulations, we concluded that the error signal extraction algorithm presented here performs well enough for the line-scan CCD-based fringe tracker to be used as a sensor for active vibration stabilization in interferometry.

## 4. Experimental Setup

As mentioned in Section 1, we integrated the active vibration stabilization system into the measurement head of the UPC-ZEBRA interferometer, which is designed to measure the segment piston in large segmented mirrors. Figures 5 and 6 show the labo-

ratory setup for the interferometer, and a detailed description is provided in Ref. 12. The UPC-ZEBRA interferometer is positioned over the intersegment simulator, a system that reproduces the contact region of two segments, thereby allowing a controlled piston to be introduced between the segments using an integrated piezoelectric transducer (PZT) actuator. It also provides fine alignment capabilities with respect to the interferometer.

To integrate the system into the measurement head of the UPC-ZEBRA interferometer without disrupting the metrological procedures, a vibration-monitoring channel in the infrared range was added to the existing metrological channel in the visible range. No active interaction with the interferometer was required.

The light source for the vibration-monitoring channel was a 10 mW laser diode emitting at 785 nm. Its light was expanded by a 4× microscope objective and coupled to the metrological beam (in the visible range of the spectrum) using a dichroic beam coupler specifically designed to work at a 45° incidence angle, which reflected almost 100% of the incident light at 785 nm and transmitted most of the light in the visible range (400–700 nm). Figure 7 shows the transmission curve we measured for this coupler.

Thus the metrological and vibration-monitoring beams shared most of the optical path inside the interferometer. At the exit of the interferometer, before the beams reached the metrological CCD area-scan camera, a beam decoupler with the same characteristics as the beam coupler (also at 45°) was used to decouple the two beams. The visible beam was transmitted, while the infrared beam was reflected at 90° and directed at the line-scan CCD camera. We chose a 1024-pixel line CCD sensor (10.2 mm side) that can be operated at up to 50,000 lines/s. Since the line CCD sensor was larger than the metrological CCD sensor (6.4 mm), reimaging optics were placed in the path of the infrared beam before it reached the line-scan CCD camera, so that both cameras would image the same region of the object plane, which simplified the alignment procedure.

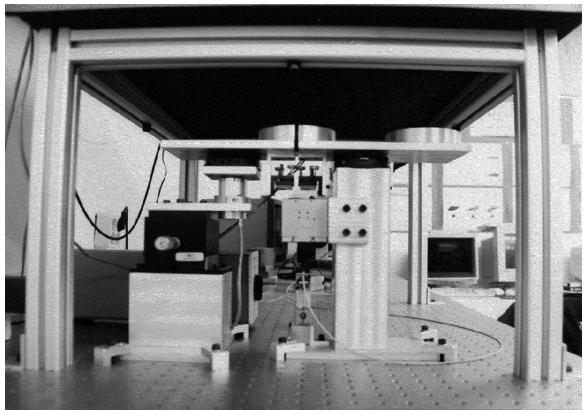

Fig. 6. Segment simulation interface located below the interferometer.

The interferograms acquired by the line-scan CCD camera were captured by a frame-grabber board inside a computer. These data were then processed using the algorithm described in Section 2, which was implemented in ASSEMBLER due to the processing speed required. We entered the output in the control algorithm implemented in C++. We analyzed several control techniques, and the one that gave the best results was a proportional integral (PI) algorithm tuned using an intervalar technique. The control stage is described in greater detail in Ref. 13. Using a 16-bit digital-to-analog converter, we then output the control signal to the actuator used to compensate for the vibration. This actuator is a PZT with a maximum travel range of 30 μm placed below the

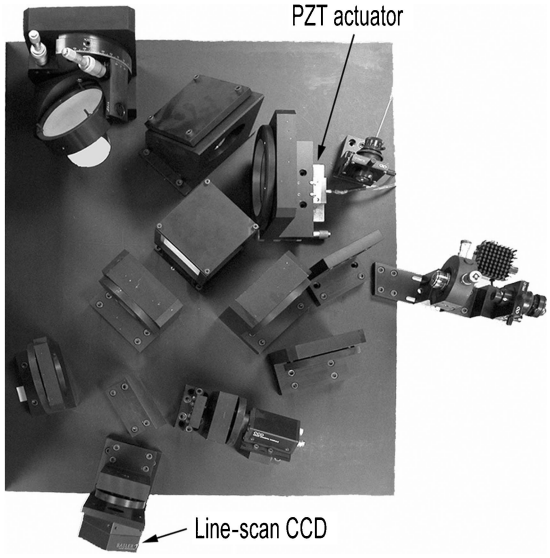


Fig. 5. General view of the UPC-ZEBRA interferometer in which several elements of the active vibration stabilization system are indicated.

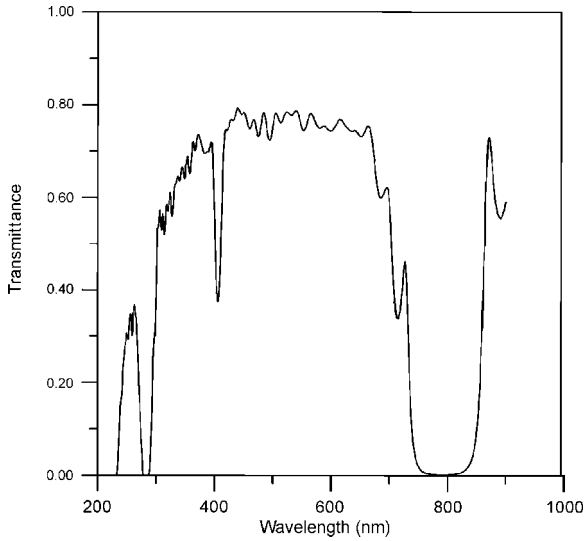


Fig. 7. Transmission curve for the beam coupler–beam decoupler, measured using a Perkin-Elmer Lambda 3B spectrophotometer (at an incidence angle of 45°).

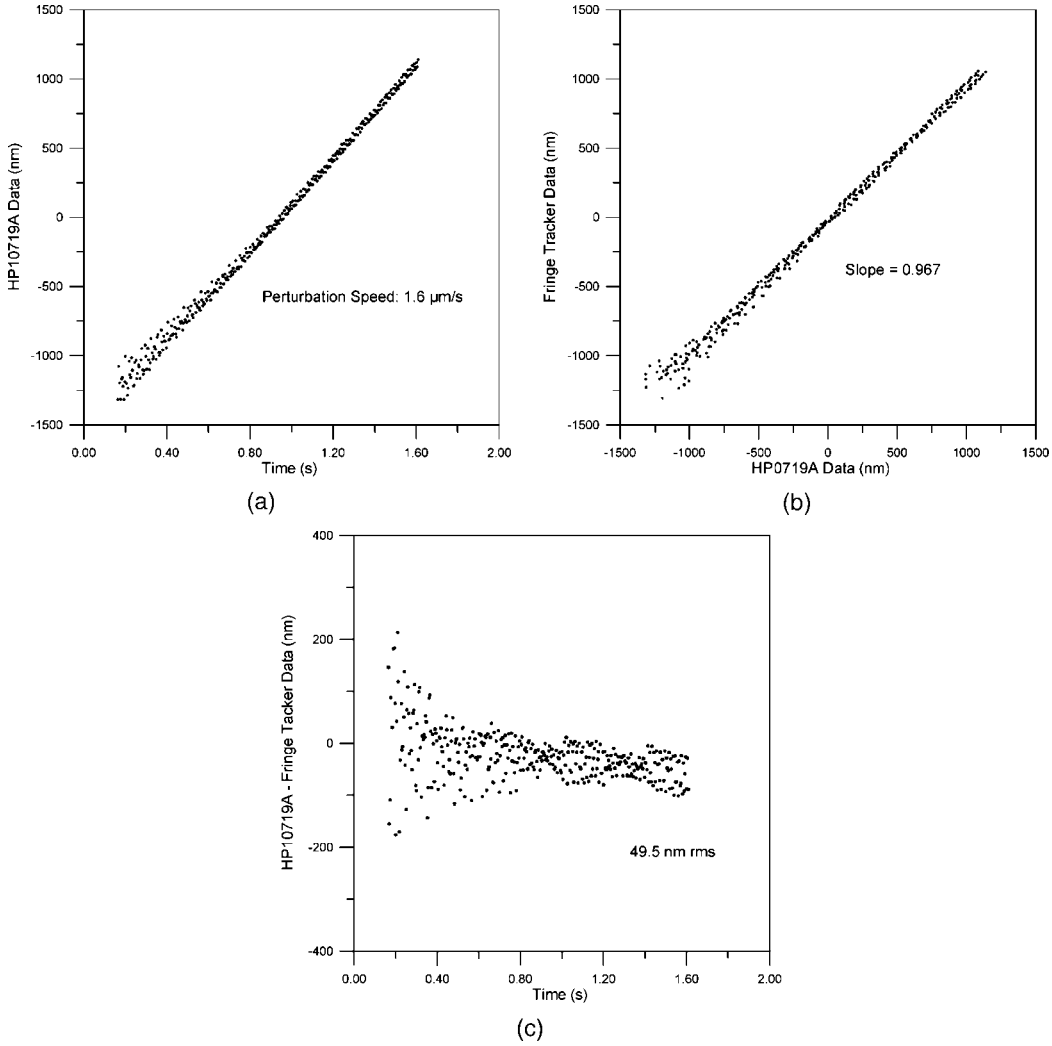


Fig. 8. Performance of fringe tracker (fringe speed, 1.6 μm/s): (a) perturbation introduced, (b) perturbation measured by the fringe tracker versus perturbation measured by HP10719A, and (c) difference between the results of the fringe tracker and HP10719A versus time.

internal mirror of the interferometer that balances the OPD.

Because the UPC-ZEBRA was tightly positioned over the intersegment simulator, we were unable to introduce a relative perturbation between them, as would occur in real conditions. Instead, to produce an equivalent effect, we positioned the line-scan camera to image an interferogram from the segment that can be moved using the integrated PZT actuator placed in the intersegment simulator. However, the travel range of this actuator is only 6 μm, which limited the tests that we could carry out in the laboratory.

### 5. Preliminary Results

We conducted tests to verify that the fringe tracker was performing properly. In these tests, we introduced a known perturbation in the system using the PZT actuator, which was placed below one of the segments in the intersegment simulator. We monitored this perturbation using a differential interferometer (HP10719A), which was also integrated into the intersegment simulator. The drawback of this setup is that only low-frequency perturbations with amplitudes of ±3 μm can be generated, as this is the maximum travel range of the PZT actuator. Therefore it was not possible to carry out large-amplitude tests in the laboratory using this setup. The low-amplitude tests were used to verify the performance of the fringe tracker. Once this has been checked, a scaling in the acquisition parameters would be needed to track fringes at larger perturbation amplitudes.

Figure 8 shows the results of the fringe-tracker performance tests when a linear perturbation of 1.6 μm/s is introduced. This was one of the perturbations that we analyzed in the simulations presented in Section 3.

Figure 8(b) shows that the measurement of the fringe tracker closely matches that of the HP10719A interferometer. This is shown more clearly in Fig. 8(c), in which the difference between the perturbation measured by the fringe tracker and that measured

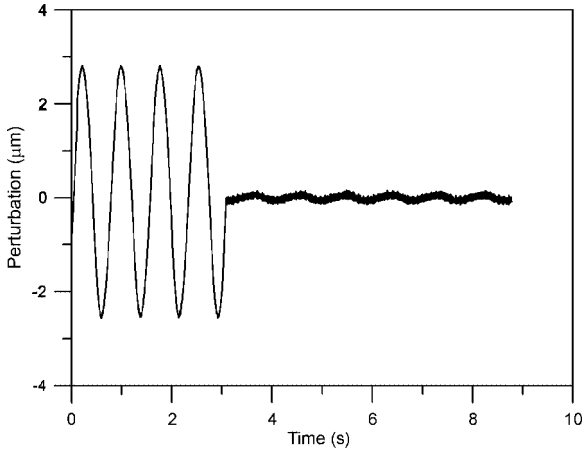


Fig. 9. Graph showing the performance of the active control system. The perturbation is reduced by a factor of 1/200 when the closed-loop system is activated.

by HP10719A is plotted over time. The average (rms) difference was 50 nm ($\lambda/15$), much less than one fringe, which is good enough for the active vibration-stabilization system to work properly. This figure was also much larger than the digital noise of the error signal extraction algorithm (6 nm, as seen in Section 3), which confirms that the introduction of digital noise did not affect the performance of the fringe tracker.

To experimentally validate the technique and the control stage,[13] different sinusoidal disturbances below 4 Hz with an amplitude of $\pm 3000$ nm were applied.

Figure 9 shows the result of the attenuation obtained when applying a sinusoidal perturbation of 1.4 Hz. The residual amplitude is approximately $\pm 15$ nm ($\lambda/50$). Therefore the attenuation obtained is a factor of 1/200, that is, $-46$ dB. This means that the system operating in the closed-loop mode will be able to maintain, by far, the zeroth-order fringe within the field of view of the area-scan CCD camera, as required by the algorithms[14] used to extract the piston error in the UPC-ZEBRA interferometer.

## 6. Conclusions

In this paper, we have introduced a new method that can be used in applications involving optical interferometers to actively compensate for mechanical perturbations. We have developed a new fringe tracker that uses a line-scan CCD and a new error signal extraction technique. We designed both of these for the UPC-ZEBRA, a large-aperture Michelson interferometer built specifically for measuring the segment piston locally in large segmented mirrors. For this application, large OPD variations ($\pm 300$ μm) at a relatively low frequency (<1 Hz) are expected because of the oscillating behavior of the mechanical system that positions the interferometer in front of each pair of segments.

We found the output of the fringe tracker to be proportional to the OPD variation (i.e., fringe velocity). It was obtained by comparing two consecutive interferograms captured by the high-frequency line-scan CCD. We also simulated the output of the fringe tracker for different perturbations, mainly linear and sinusoidal, and the tracking algorithms performed well.

We integrated the fringe-tracking device into the experimental setup of the UPC-ZEBRA interferometer using an infrared monitoring channel in addition to the visible piston-measurement channel. We introduced the output of the fringe tracker as the error signal into a control system, which used a PI algorithm tuned by using an intervalar technique. We closed the control loop by feeding the control signal to a PZT actuator that positions an internal mirror, which balances the OPD variations. The preliminary experimental results we obtained with linear perturbations of 1.6 μm/s showed that the system is able to track fringes with an average rms error close to 50 nm (much less than one fringe) when operating in the open-loop mode. When the loop is closed, low-frequency sinusoidal perturbations of amplitude $\pm 3000$ nm are attenuated by a factor of 1/200. This confirms that such a system is suitable as a perturbation sensor for actively stabilizing vibrations in the UPC-ZEBRA interferometer.

The authors thank the Comisión Interministerial de Ciencia y Tecnología for providing part of the funding for this research. A. Pintó also thanks the Department of Universities, Research and the Information Society of the Generalitat de Catalunya for the Ph.D. grant he received, which enabled him to take part in this study.

## References

1. F. Barone, R. De Rosa, L. Di Fiore, F. Fusco, A. Grado, L. Milano, and G. Russo, "Real-time digital control of optical interferometers by the mechanical-modulation technique," Appl. Opt. **33,** 7846–7856 (1994).
2. F. Barone, E. Calloni, L. Di Fiore, A. Grado, L. Milano, and G. Russo, "Digital error-signal extraction technique for real-time automatic control of optical interferometers," Appl. Opt. **34,** 8100–8105 (1995).
3. J. L. Camp, L. Sievers, R. Bork, and J. Heefner, "Guided lock acquisition in a suspended Fabry–Perot cavity," Opt. Lett. **20,** 2463–2465 (1995).
4. G. W. Neat, J. W. Melody, and B. J. Lurie, "Vibration attenuation approach for spaceborne optical interferometers," IEEE Trans. Control Syst. Technol. **6,** 689–700 (1998).
5. G. Cole, J. H. Burge, and L. R. Dettman, "Vibration stabilization of a phase-shifting interferometer for large optics," in *Optical Manufacturing and Testing II,* H. P. Stahl, ed., Proc. SPIE **3134,** 438–446 (1997).
6. I. Yamaguchi, J. Liu, and J. Kato, "Active phase-shifting interferometers for shape and deformation measurements," Opt. Eng. **35,** 2930–2937 (1996).
7. M. E. Germain, "Intensified CCD fringe tracker," in *Interferometry in Optical Astronomy,* P. J. Léna and A. Quirrenbach, eds., Proc. SPIE **4006,** 1029–1034 (2000).
8. S. Morel, W. A. Traub, J. D. Bregman, R. Mah, and E. Wilson, "Fringe-tracking experiments at the IOTA interferometer," in *Interferometry in Optical Astronomy,* P. J. Léna and A. Quirrenbach, eds., Proc. SPIE **4006,** 506–513 (2000).
9. L. Koechin, P. R. Lawson, D. Mourard, A. Blazit, D. Bonneau, F. Morand, Ph. Stee, I. Tallon-Bosc, and F. Vakili, "Dispersed

fringe tracking with the multi-$r_o$ apertures of the Grand Interféromètre à 2 Télescopes," Appl. Opt. **35,** 3002–3009 (1996).
10. A. Pintó, "New interferometric technique for piston measurement and phasing of segmented mirrors," Ph.D. dissertation (Universitat Politècnica de Catalunya, Barcelona, Spain, 2002).
11. C. Pizarro, J. Arasa, F. Laguarta, N. Tomas, and A. Pintó, "Design of an interferometric system for the measurement of phasing errors in segmented mirrors," Appl. Opt. **41,** 4562–4570 (2002).
12. A. Pintó, F. Laguarta, R. Artigas, and C. Cadevall, "Testing and applicability of the UPC-ZEBRA interferometer as a phasing system in segmented-mirror telescopes," Appl. Opt. **43,** 1091–1096 (2004).
13. R. Comasòlivas, T. Escobet, J. Quevedo, A. Pintó, F. Laguarta, and J. Vicente are preparing a paper to be called "Active control based on QFT for vibration attenuation in optical interferometers."
14. A. Pintó, F. Laguarta, R. Artigas, and C. Cadevall, "New interferometric technique for piston measurement in segmented mirrors," J. Opt. A, Pure Appl. Opt. **4,** 369–375 (2002).